RC2: 'Comment on gmd-2024-51', Anonymous Referee #2, 21 Oct 2024

The manuscript introduces AI-NAOS, an AI-based module that incorporates nonspherical and inhomogeneous aerosol particles into radiative transfer simulations. The use of deep learning and advanced optical modeling is an innovative approach in this field, significantly improving accuracy in predicting the direct radiative effects of aerosols. Real-case simulations provide substantial evidence of the AI-NAOS module's impact on atmospheric thermodynamic structures and precipitation patterns, enhancing the understanding of aerosols in weather modeling. In general, the manuscript is well-organized. Only minor revision is needed before publication:

Response: We appreciate the reviewer's positive comment on this study and constructive suggestions for improving the manuscript.

The model ran for 72 hours starting from January 12, 2018, with only 24 hours of spin-up time, which seems rather short. Is it possible to extend the model's spin-up time and total run time?

Response: Thanks for your suggestion. Currently, we are integrating the module into the CESM2/CAM6 climate model, in which case we will increase the run time for tests as needed. For the weather-scale case studied here, while the spin-up and total run time can be extended for additional analysis, we believe that the chosen spin-up and total run time of 24 hours and 72 hours, respectively, are adequate for our purposes.

It is worth noting that a spin-up time of 12 hours is commonly used in mesoscale numerical weather prediction models (Dzebre et al., 2019; Wang et al., 2021). For certain initial conditions with disturbing weather events, a longer spin-up time may be required. In our case with no disturbing weather events, the 24-hour spin-up was sufficient for the model to reach a physical equilibrium state (Liu et al., 2023).

Regarding the total run time, studies have indicated that a duration ranging from 1 day to 5 days is acceptable in a weather-scale case study(Di et al., 2015; Iguchi et al., 2012). Given the current configuration of our model and the short time available for manuscript revision, we have not extended the run time for further analysis.

Is 'deep neural network (DNN)' used in the text as a general term for a class of methods, or does it refer to a specific neural network method? Please clarify this further in the text.

Response: Thank you for raising this question for clarification. DNN is used in the text as a general term referring to a series of neural networks with multiple hidden layers. However, in the context of this study, we specifically employ a multiple-target DNN that was developed in Wang et al. (2023). To provide further clarification, we have updated the manuscript with following inclusions (Line 181):

A multiple-target DNN model that has been designed to infer the single-scattering properties of encapsulated fractal aggregates of BC was adapted to bulk optical properties inference in this study.

Why were different methods chosen for shortwave radiation and longwave radiation? I believe that RRTM can also be used for shortwave calculations. What considerations influenced this decision?

Response: The use of different methods for shortwave and longwave radiation was based on the specific configurations and developments within the GRAPES_Meso5.1/CUACE model (Peng et al., 2022). We decided to maintain this configuration for consistency and simplicity. We understand that there are alternative approaches and configuration. We appreciate your insights for future considerations.

Could you compare it with the latest research on non-spherical black carbon, such as the study by Chen, G., Liu, C., Wang, J., Yin, Y., & Wang, Y., JGRA, 2024, which accounts for the mixing state, nonsphericity, and heterogeneity effects of black carbon in its optical property parameterization within a climate model?

Response: Thanks for the reviewer's comment. Chen et al. in their study published in JGRA have indeed made significant progress by establishing a 3-D dataset of bulk optical properties of non-spherical black carbon and integrating it into the climate model CAM6 using a look-up table method. Their work effectively addresses the overestimation of BC absorption by considering particle nonsphericity.

The primary difference between Chen's work and our NAOS framework are twofold:

Firstly, the database employed differ significantly. In our research, we use the IITM algorithm to create our database, which offers a more efficient and accurate alternative to the discrete dipole approximation (DDA) method used by Chen et al. Thus, our database is larger and more comprehensive. For example, Chen's 3-D database includes only a single value of complex refractive index (RI) of BC and consider just two values for the real part and two for the imaginary part of RI for coating materials. Additionally, the size range of BC particles is limited, leading to the use of spherical core-shell models for large bins in their dataset. This limitation means that the nonsphericity of large BC particles in accumulation mode and all BC particles in primary carbon mode have not been accounted for.

Secondly, the look-up table method necessitates interpolation, which may introduce non-negligible numerical errors, especially when interpolating points are sparse. In contrast, the DNN approach provides continuous predictions, outperforming traditional interpolation. While both studies apply similar encapsulated fractal aggregates models, Chen's work includes a more diverse range of shapes. Similarly, we plan to incorporate additional shapes with varying fractal dimensions into our NAOS framework in future updates.

I believe there is still considerable uncertainty regarding the impact on precipitation in this section. It's worth further consideration whether to include this in the article. Additionally, while not absolutely necessary, it might be beneficial to examine changes in the boundary layer as well.

Response: Thanks for your valuable feedback. We acknowledge the complexity of the relationship between DRE and precipitation, particularly in extreme weather scenarios. In our study, which focused on light winter rainfall, the suppression effect on precipitation can primarily be attributed to reduced convection due to decreased boundary layer height.

To further elucidate this mechanism, we have conducted a detailed examination of boundary layer height and incorporated a new subfigure in Figure 11. Additionally, Section 3.5 has been revised accordingly:

Figure 11 depicts the anomalies in height of PBL and accumulated precipitation over the last 48 hours, comparing the AI-NAOS scheme with a control scheme of zero AOD. The analysis focused on a specific region (101.5-112.5°E, 29.5-34.5°N), encompassing parts of the Sichuan Basin and the Middle Yangtze Plain. The results indicate a suppression effect on precipitation accompanied by a decrease in PBL height in this region. The spatially averaged precipitation anomaly was -0.24 mm for the AI-NAOS module, with anomalies of -0.21, -0.26, and -0.27 mm for the external-mixing, core-shell, and volume-mixing schemes, respectively. The PBL height anomalies for AI-NAOS and the three spherical schemes were -56.8, -48.7, -63.0, and -64.4 meters, respectively. Notably, the suppression effect was less significant in the external-mixing scheme. The NSIH effect amplified the suppression effect by approximately 15%. In the core-shell and volume-mixing schemes, this effect was even more pronounced, similar to the thermodynamic effect. Despite the complexity of aerosol-precipitation relationship, the suppression effect observed in our study can be attributed primarily to the aerosol-induced stability leading to weaker convection, as evidenced by the changes in the PBL height.

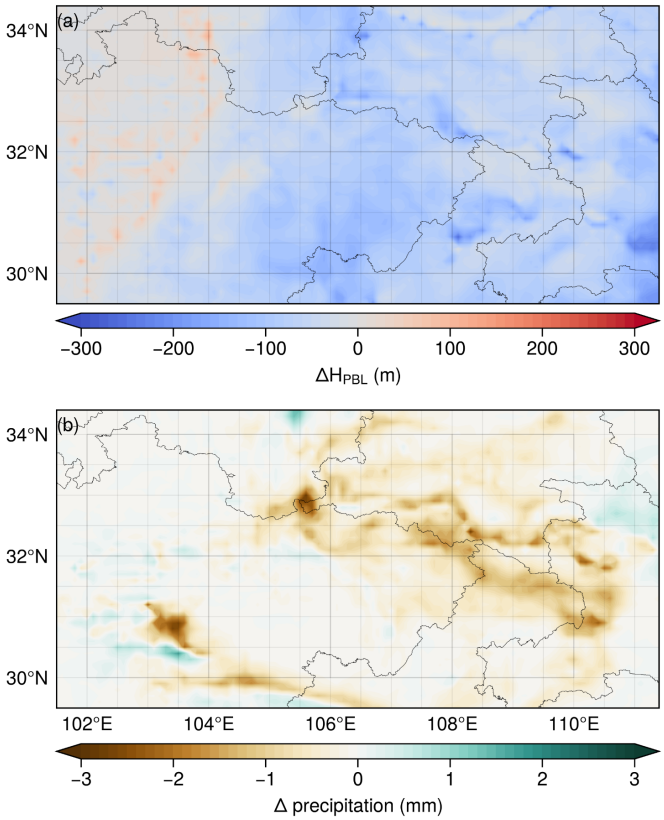

Figure 11. Anomalies in (a) height of planetary boundary layer and (b) accumulative precipitation between the AI-NAOS module and the control scheme over a specific region within the precipitation center (101.5–112.5°E, 29.5–34.5°N).

Some minor comments:

In Line 40, omega is used to represent SSA, while in Line 271, <SSA> is used. Please ensure consistency. The same applies to the asymmetry factor.

Response: The omega symbol was used to represent SSA of single particle while <SSA> was used to represent bulk SSA. These two variables were represented by two different symbols and the relationship was described in Eq. 7.

$$< SSA > = \frac{\int_{D_{min}}^{D_{max}} \omega q_{ext} D^2 n(D) dD}{\int_{D_{min}}^{D_{max}} q_{ext} D^2 n(D) dD} , \quad (7)$$

Line 80: It is usually referred to as 'WRF-Chem' rather than 'WRF/chem'.

Response: Corrected. Thanks.

The vertical axis of Figure 6b is labeled 'atmo. abs.', which seems less rigorous than 'DRE'.

Response: Thanks! After some considerations, we decided to use ‘'Atmo. Abs.’ for better understanding since the difference of net solar flux between TOA and surface could be totally attributed to absorption rather than scattering.

Section 3.4 appears twice; the precipitation part should be labeled as 3.5.

Response: Corrected. Thanks!

References:

Di, Z., Duan, Q., Gong, W., Wang, C., Gan, Y., Quan, J., Li, J., Miao, C., Ye, A., and Tong, C.: Assessing WRF model parameter sensitivity: A case study with 5 day summer precipitation forecasting in the Greater Beijing Area, Geophysical Research Letters, 42, 579–587, https://doi.org/10.1002/2014GL061623, 2015.

Dzebre, D. E. K., Acheampong, A. A., Ampofo, J., and Adaramola, M. S.: A sensitivity study of Surface Wind simulations over Coastal Ghana to selected Time Control and Nudging options in the Weather Research and Forecasting Model, Heliyon, 5, e01385, https://doi.org/10.1016/j.heliyon.2019.e01385, 2019.

Iguchi, T., Matsui, T., Tokay, A., Kollias, P., and Tao, W.-K.: Two distinct modes in one-day rainfall event during MC3E field campaign: Analyses of disdrometer observations and WRF-SBM simulation, Geophysical Research Letters, 39, https://doi.org/10.1029/2012GL053329, 2012.

Liu, Y., Zhuo, L., and Han, D.: Developing spin-up time framework for WRF extreme precipitation simulations, Journal of Hydrology, 620, 129443, https://doi.org/10.1016/j.jhydrol.2023.129443, 2023.

Peng, Y., Wang, H., Zhang, X., Zheng, Y., Zhang, X., Zhang, W., Liu, Z., Gui, K., Liu, H., Wang, Y., and Che, H.: Aerosol-radiation interaction in the operational atmospheric chemistry model GRAPES_Meso5.1/CUACE and its impacts on mesoscale NWP in Beijing-Tianjin-Hebei, China,

Atmospheric Research, 280, 106402, https://doi.org/10.1016/j.atmosres.2022.106402, 2022.

Wang, X., Tolksdorf, V., Otto, M., and Scherer, D.: WRF-based dynamical downscaling of ERA5 reanalysis data for High Mountain Asia: Towards a new version of the High Asia Refined analysis, International Journal of Climatology, 41, 743–762, https://doi.org/10.1002/joc.6686, 2021.

The following are additional revisions:

1. Figure 1 were displayed in another viewing angle for better understanding.

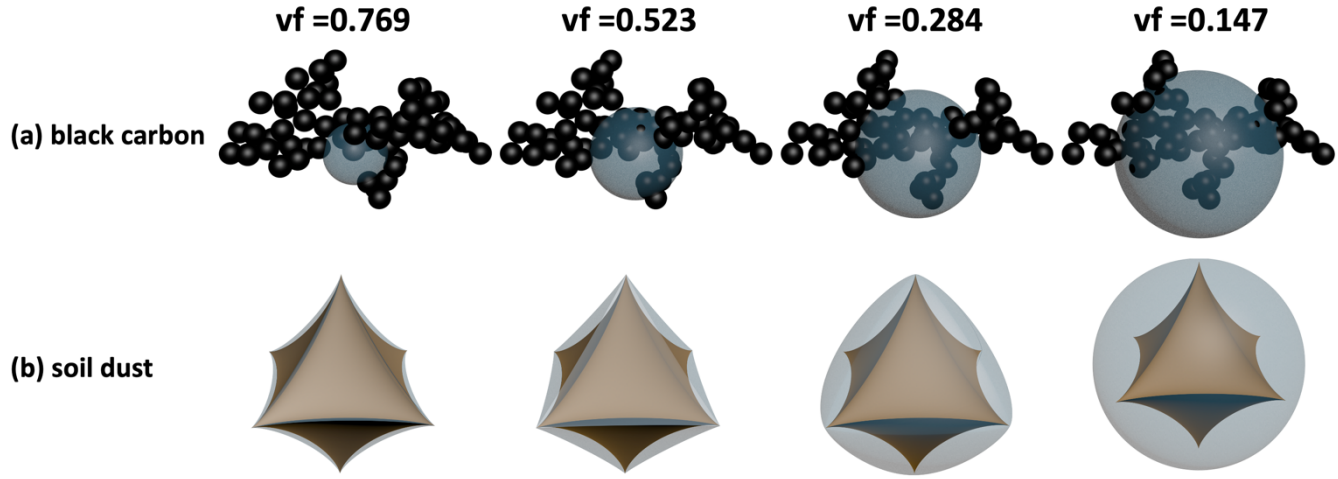

Figure 1. Optical modelling for (a) fractal aggregates framework of black carbon (BC) partially encapsulated with spherical coating of hygroscopic aerosols and (b) super-spheroid framework of soil dust (SD) fully coated with another super-spheroid of hygroscopic aerosols with various volume fractions.

2. A figure was added to illustrate the framework of AI-NAOS module (Figure 2).

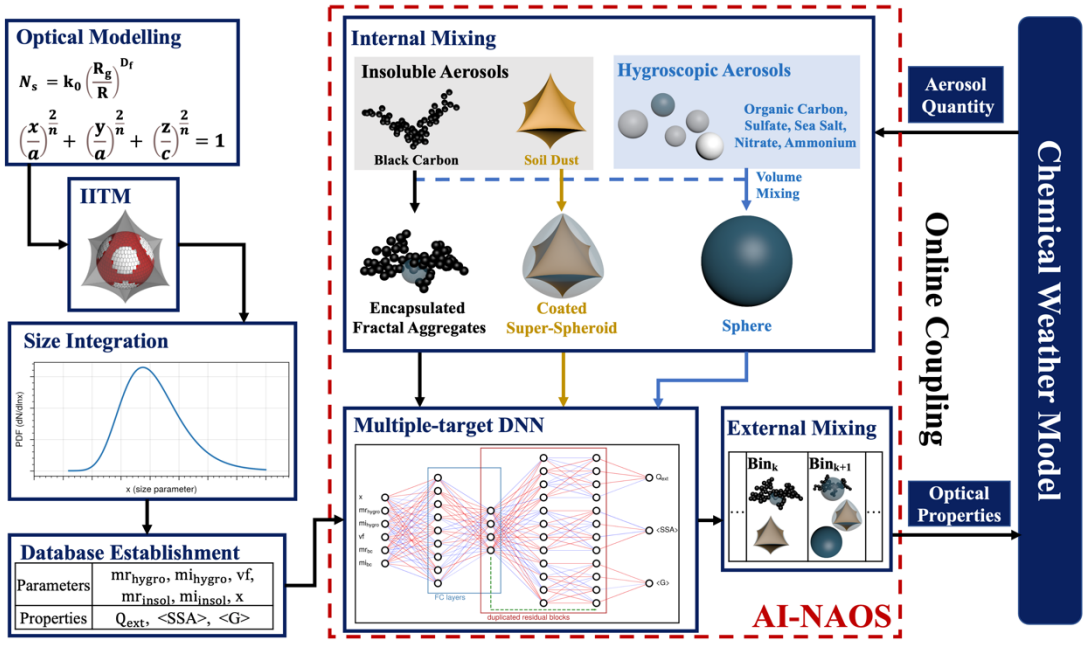

Figure 2. The framework of AI-NAOS module.

3. Figure 10 was modified. Pressure levels ranged from 700 hPa to the surface instead of 1000 hPa in the new version and vertical averaged values were corrected. The main conclusion, "The NSIH effect could enhance the short-wave heating rate, reaching 20%", was changed to "The NSIH effect could enhance the short-wave heating rate, reaching 23%".

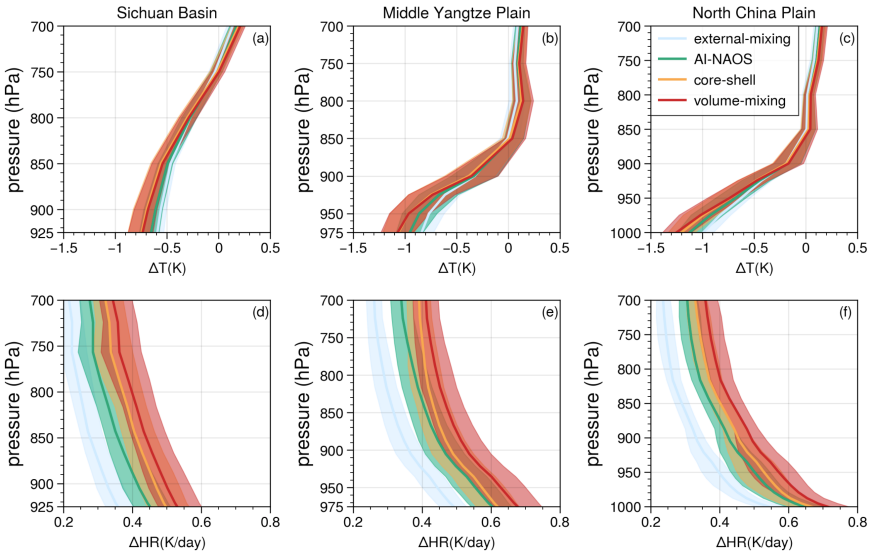

Figure 10. Vertical profiles of (a-c) temperature and (d-f) short-wave heating rate anomalies based on four aerosol optical schemes (external-mixing, AI-NAOS, core-shell, and volume-mixing). The solid lines represent the median value and the shaded areas encompass the range from the 25 to 75 percentage.

4. The color schemes were modified in Figure 3, 7, 8, 10, for the convenience of readers with color vision deficiencies.

5. The repository for GRAPES_Meso5.1/CUACE was added (Line 585)
The repository for GRAPES_Meso5.1/CUACE developed by Wang et al., 2022a, is in Zenodo (https://zenodo.org/records/7075751).